

Your Paper's Title Starts Here: Please Center Your Paper's Title Starts Here: Please Center

Toby XXX¹, Caesar XXX^{2,*}

¹ Hong Kong University of XXX, Kowloon, Hong Kong

² Rensselaer XXX Institute, Troy, New York, 12180, USA

* Corresponding Author

Abstract

This template explains and demonstrates how to prepare your camera-ready paper for Trans Tech Publications. The best is to read these instructions and follow the outline of this text. Please make the page settings of your word processor to A4 format (21 x 29,7 cm or 8 x 11 inches); with the margins: bottom 1.5 cm (0.59 in) and top 3 cm (1.18 in), right/left margins must be 2 cm (0.78 in). This template explains and demonstrates how to prepare your camera-ready paper for Trans Tech Publications. The best is to read these instructions and follow the outline of this text. Please make the page settings of your word processor to A4 format (21 x 29,7 cm or 8 x 11 inches); with the margins: bottom 1.5 cm (0.59 in) and top 3 cm (1.18 in), right/left margins must be 2 cm (0.78 in).

Keywords

List the; keywords covered; in your paper

1 Introduction

Many experiments have been undertaken to investigate the film rupture process [1-6]. At the first stage of liquid film drainage when a relatively thick liquid phase exists between air bubbles, gravity plays an important role. When the thickness decreases to ~100 nm, the gravity effect becomes negligible, and interfacial interactions including electrostatic, dispersion, and hydration forces begin to be major factors in film drainage and rupture.

The experiment is accumulative result of many environmental effects [7-14]: random motion of microscopic particles, collisions of surrounding gas molecules, atmospheric humidity etc. Experiments [11] using microinterferometry showed that foam films of ultrapure de-ionized (DI) water can last up to 10 s, and the contact time between two gas bubble surfaces at close proximity significantly influences the film drainage, rupture, and lifetime. Also using microinterferometry, Karakashev *et al.* [7] reported the effects of ions on film rupture and the lifetime of aqueous foam films formed from sodium chloride (NaCl), lithium chloride (LiCl), sodium acetate (NaAc),

and sodium chlorate (NaClO_3). They found that relatively long-lasting and non-draining films prepared from salt solutions above 0.1 M could be observed. The film lifetime was significantly longer by 1 to 2 orders-of-magnitude (i.e., from 10 to 100 s). Also, both the film lifetime and the (average) thickness of the non-draining films increased with increasing salt concentration. This effect has not been observed with foam films stabilized by surfactants. The film lifetime and thickness also increased with increasing film radius. From all these experiments, the thickness order was usually ~ 100 nm, which is a very different value from the thicknesses obtained using computer simulations.

Recent experiments [15, 16] suggested that nanobubbles can stably form at a hydrophobic surface and in an aqueous solution, and can be used to explain the liquid film rupture through a number of stages [17, 18]. For example, during the film drainage between a big air bubble and a hydrophobic surface, the macroscopic bubble first approaches the apex of the largest surface nanobubbles. An aqueous foam film in nanometer size is effectively formed between the macroscopic bubble and the nanobubble, where the van der Waals attraction is strong. The attractive van der Waals force can destabilize the film locally as traditionally proposed [19]. The local film destabilization can be further increased by the increase in the local capillary pressure due to the concave surface of the nanobubble, causing the disappearance of the entire macroscopic film. Understanding the rupture of the nanofilms is critical to the nanobubble theory on the rupture of macroscopic films. Unfortunately, the nanofilms cannot be directly visualized and examined due to the limit of optical resolution available. Therefore, studies of nanofilm rupture by MD simulation would be extremely useful in this regard.

Computer simulations and experimental measurements have been used widely in attempts to understand chemical phenomena in bulk liquids, liquid/air, liquid/liquid and liquid-solid interfaces [20-29]. Understanding liquid film systems are important in understanding industrial processes such as phase separation, flotation separation of particle using gas bubbles, water desalination, etc. Aqueous film systems could be classified mainly as water films containing ions or liquid films containing surfactants. From the perspective of MD simulations, and given the experimental complications associated with the studies of thin films, it makes sense to combine experimental approaches with computational studies to discover new insights that can be used to interpret the fundamental aspect of the phenomena. In this research we present a new model — critical rupture time (CRT) — and propose new criteria for defining and determining the critical thickness and CRT of the film, which, in turn, could be used to accurately distinguish the rupture point based on user-selected parameters. We used the Gibbs dividing area, two stable states, and the correlation between CRT and critical thickness of the aqueous film to predict the critical thickness and CRT. Then, using pure water film as a reference, we determined the effect of ions on the film rupture process. The results from our simulations also were compared with results from experiments.

2 Molecular Models and MD Parameters

OPLS-AA (all-atom optimized potentials for liquid simulations) force field was applied in this study with periodic boundary conditions in three dimensions. Total energy was the sum of potential energy and kinetic energy. Total potential energy contained: bonded interactions, including bond E_{bond} , angle E_{angle} , and torsion

interactions $E_{torsion}$; and non-bonded interactions $E_{nonbond}$, including van der Waals and Coulombic interactions. The equations were as follows,

$$E_{bond} = \sum_{bonds} K_r (r - r_{eq})^2$$

$$E_{angle} = \sum_{angles} K_\theta (\theta - \theta_{eq})^2$$

$$E_{torsion} = \sum_i \frac{V_1}{2} [1 + \cos(\phi_i)] + \frac{V_2}{2} [1 - \cos(2\phi_i)] + \frac{V_3}{2} [1 + \cos(3\phi_i)]$$

Here, r_{eq} , θ_{eq} are equilibrium values of the bond length and bond angle.

$$E_{nonbond} = \sum_{i < j} \left[4\epsilon_{ij} \left(\frac{\sigma_{ij}^{12}}{r_{ij}^{12}} - \frac{\sigma_{ij}^6}{r_{ij}^6} \right) + \frac{q_i q_j}{r_{ij}} \right] f_{ij}$$

The geometric combining rules (OPLS) for the Lennard-Jones coefficients were employed as

$$\epsilon_{ij} = (\epsilon_{ii} \epsilon_{jj})^{1/2}; \sigma_{ij} = (\sigma_{ii} \sigma_{jj})^{1/2}$$

The coefficient $f_{ij} = 0.0$ for any i - j pairs connected by a valence bond (1-2 pairs) or a valence bond angle (1-3 pairs); $f_{ij} = 0.5$ for 1-4 pairs interactions (atoms separated by exactly three bonds) and $f_{ij} = 1.0$ for all of the other cases.

2.1 Molecular models and MD parameters

MD simulations were performed using the *GROMACS* software package 4.5.3 [30-33]. In addition, the ion parameters used were specified within the OPLS-AA force field, which were in the data files corresponding to the *GROMACS* distribution. The MD model for water was a simple extended point-charge model as it could reproduce thermodynamic properties at a relatively low computational cost. In the future work, we will employ potential models that taking many-body effects into account. Long-range electrostatic interactions were treated by the particle mesh Ewald. The Lennard-Jones and Coulombic interactions both had a real space cut-off fixed at 14 Å. All simulations were undertaken at a time step of 1 fs. Time coupling used the v-rescale method at a constant temperature of 300 K with a time coupling of 0.1 ps. The velocity-rescaling thermostat is essentially a Berendsen thermostat, which can produce a correct canonical ensemble and still has the advantage of the Berendsen thermostat.

2.2 Simulation procedure

We first created the film using *GROMACS* by defining the lateral scale ($L_x=L_y$) and the thickness of film in three dimensions. We then put the film at the centre of a vacuum box ($L_x=L_y=L_z/3$) to simulate the liquid-vapour interface. A slab geometry was employed as follows: the size of the box was set to $L_x=L_y$, $L_z=3 L_x$; the lateral sizes ($L_x=L_y$) of film had the same value as the lateral dimensions of the box, and the Z -dimension of the film was centred in the box with the two surfaces perpendicular to the Z -axis. The overall packing of water films for the initial configuration was close to the experimental density of water (1000 kg m^{-3}).

Some water molecules could escape from the water layer during the simulation. The water molecules and ions were randomly packed into their corresponding boxes. The run times were 11 ns for most water films, 11 ns for films with ions in critical thickness range (Gibbs dividing range in Part 3.3), and 3 ns for films with ions not in

Gibbs dividing range. The first 500 ps were used as equilibration period in the NVT ensemble. For water films, five lateral sizes (3×3 , 4×4 , 6×6 , 8×8 , 10×10 nm) and 10 simulation durations (1-10 ns) were chosen to study the simulation results. The film L_z value ranged from 0.7 to 1.5 nm. For films with Na^+ and Cl^- ions, the 3×3 nm film contained 8 ions, the 4×4 nm film contained 15 ions, and the 6×6 nm film contained 30 ions. The critical thickness could be determined from the density profile results, and CRT can be obtained by studying the certain size of a film, which ran for 11 ns, applying density, and combining with trajectory snapshots to judge the rupture.

3 Results and Discussions

3.1 From thin film rupture process to define CRT

3.1.1 Introduction for the criteria of critical density percentage

To introduce CRT, $4 \times 4 \times 1.05$ and $4 \times 4 \times 1.10$ nm water films were selected as examples to illustrate this methodology. When defining the CRT, the dimensions of the film should be fixed ($L_x=L_y$, L_z , all fixed) and the water density inside the film versus run time of MD simulation was monitored and assessed.

Table 1 (Maximum) density (kg m^{-3}) of water films versus run time.

Run time, ns	Film dimensions ($L_x \times L_y \times L_z$), nm^3	
	$4 \times 4 \times 1.05$	$4 \times 4 \times 1.10$
0.5-1	998.77	1006.60
1	997.85	1001.04
2	731.91	1000.90
3	697.14	905.50
4	570.59	733.01
5	575.13	745.72
6	576.58	748.03
7	567.37	741.03
8	572.44	750.67
9	571.33	746.73
10	574.13	749.70

0.5-1 means the data was collected from 500 - 1000ps duration, and 1 means that data was collected from 1000 to 2000 ps, etc.

Shown in Table 3-1 are the typical results for the maximum density along the Z dimension as collected at different run times. A density data file is provided as Supporting Information to show the density profile. All the density profiles were collected along the Z-axis with the box size L_z partitioned into 200 parts to calculate density; here L_z is a box size of the Z dimension, not the film thickness.

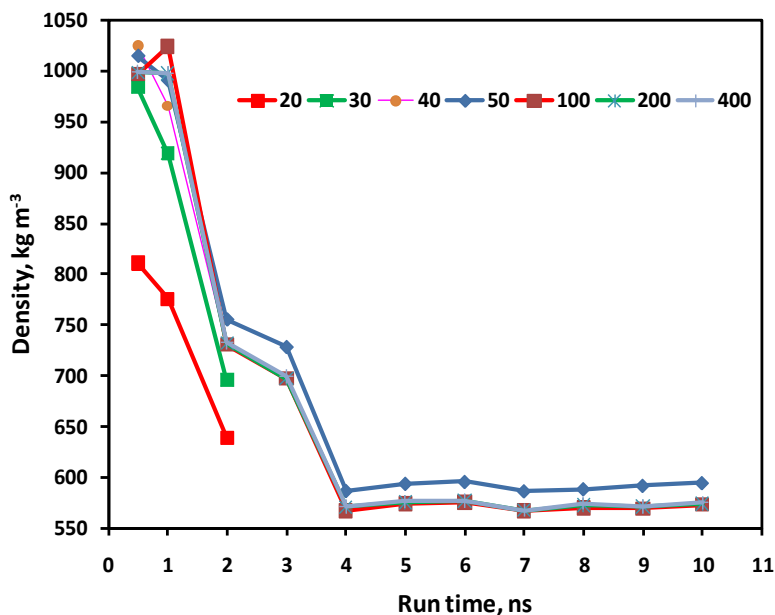


Figure 1 Effect of the number of box partitions along Z-dimension on the transient profile of (maximum) density for $4 \times 4 \times 1.05$ nm water film. The legend shows the number of partitions of the simulation box.

Figure 3-1 shows the density profiles versus the number of box partitions along the Z dimension for the $4 \times 4 \times 1.05$ nm water film. It is evident from Figure 3-1 that, if the number of box partitions is not greater than 50, the collected density cannot represent the real density profile correctly. Likewise, if the L_z were too large, 50 partitions would be unsuitable. When the number of box partitions are ≥ 100 (e.g., 200 or 400), the simulation provides a consistent density trend. Therefore, 200 box partitions were used for our simulation. As shown from the data in Table 3-1, the density decreases with increasing the run time and the density does not change significantly at long run time, for example, the density of the $4 \times 4 \times 1.05$ nm film fluctuates around ~ 570 kg m⁻³ after 4 ns.

Figure 3-2 shows snapshots of a $4 \times 4 \times 1.10$ nm water film from the unbroken state to the ruptured film state. Holes are stochastically formed within a film, but can further expand, leading to the film rupture, or collapse. The criterion then should be chosen to define CRT. Generally, the film rupture starts with the formation of a hole. Therefore, direct evidence of film rupture could be obtained by identifying a hole within a film from the snapshots and the trajectory of the system. However, more accurate evidence could be achieved from the density profile.

For the $4 \times 4 \times 1.10$ nm water film, an average density of 905.50 kg m⁻³ was obtained at 3 to 4 ns. The snapshot taken at 3700 ps (Figure 3-2) shows that the water film was not intact (as a reference, the time point at 2900 ps could be regarded as intact) even though the maximum density was 905.50 kg m⁻³. Holes were present in the film; no droplets had formed at 3-4 ns. So, even though the density was > 900 kg m⁻³, the water film can still have holes. If a film has holes, it is broken to some degree, but it is not entirely broken for droplets to form. Therefore, from the density profile of the $4 \times 4 \times 1.10$ nm water film and the snapshots in Figure 3-2, we concluded that, if the density is < 900 kg m⁻³, the film is not intact.

To extend the application of this methodology to other liquid films (e.g., H-bonding molecular films such as ethanol and polyalcohol, or non-H-bonding molecular films such as aldehydes and ketones), the intact film can be set as having 100% liquid density, and the un-intact film as a lower percentage (e.g., 90%, 80%, 60%, etc.) according to the responding condition, which will be a user-selected parameter to define its critical value according to specific purpose. The choice of this percentage (a standard of critical value, e.g., 90%, 80%, 60%, etc.) for this parameter depends on the final goal of the research, which can be input for the next modeling step (e.g., the bubble coalescence or bubble-particle attachment, the ageing process of aqueous foams [several stages can be distinguished in the foam lifetime]), etc.

With different research goals, different critical density percentages can be used to define the CRT. To study the phenomena associated with the film at the early rupture stage, one can select 90%; however, if area of interest is the middle phase, 75% might be chosen. Finally, if the goal is to investigate the influence or result of the droplets, 60% (i.e., a film that has severely broken into droplets) could be the choice.

In our research, we were concerned with the beginning of the rupture, so 90% was selected to define the CRT. We chose 900 kg m^{-3} as the standard critical density value for defining the CRT even though the choice was somewhat arbitrary. We also could have chosen 901 or 899 kg m^{-3} as the critical density for determining the CRT. However, if the average density at a certain time duration (e.g., between the n and $n+1$ steps of run times [ns]) was $> 900 \text{ kg m}^{-3}$ but $< 950 \text{ kg m}^{-3}$, the film is considered to be broken to some degree. Early in this 1-ns duration simulation, the film may be intact, however, later in the simulation, holes formed in the water film. Therefore, if the average density was below 850 kg m^{-3} , the film would be considered to be broken at the end of the 1-ns simulation.

3.1.2 Illustration for the determination of CRT

The data presented in Table 3-1 show that, after the film ruptured, the density fluctuates at a level. So, using a $4 \times 4 \times 1.10 \text{ nm}$ water film as a typical example, the CRT should satisfy the following two requirements:

1. At a 4-ns duration, the density should be $< 90\%$ (900 kg m^{-3}).
2. At a 4-ns duration, the density should be $< 90\%$ (900 kg m^{-3}) for the first time.

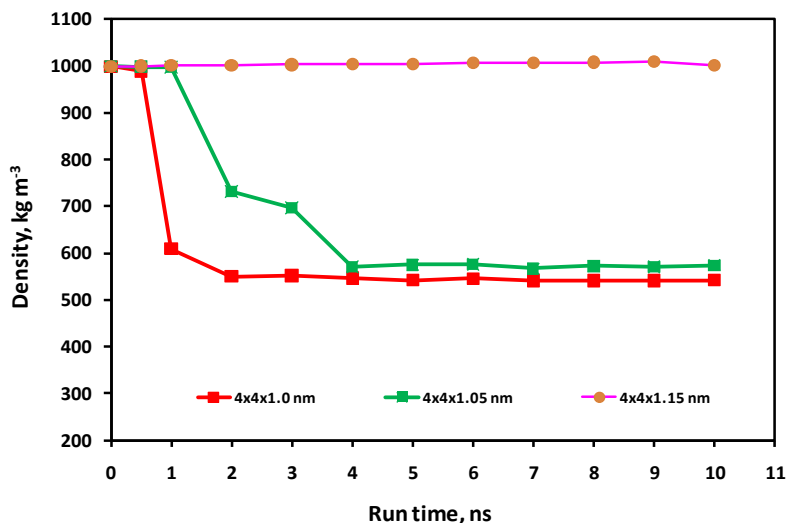


Figure 2 Typical density plots to introduce CRT: density of lateral size 4×4 nm films versus run time. The CRT for the $4 \times 4 \times 1.100$, $4 \times 4 \times 1.105$ and $4 \times 4 \times 1.15$ nm films are approximately 1 ns, 2ns and infinity, respectively.

In Figure 3-3, we show a typical plot to introduce CRT using lateral size 4×4 films as an example.

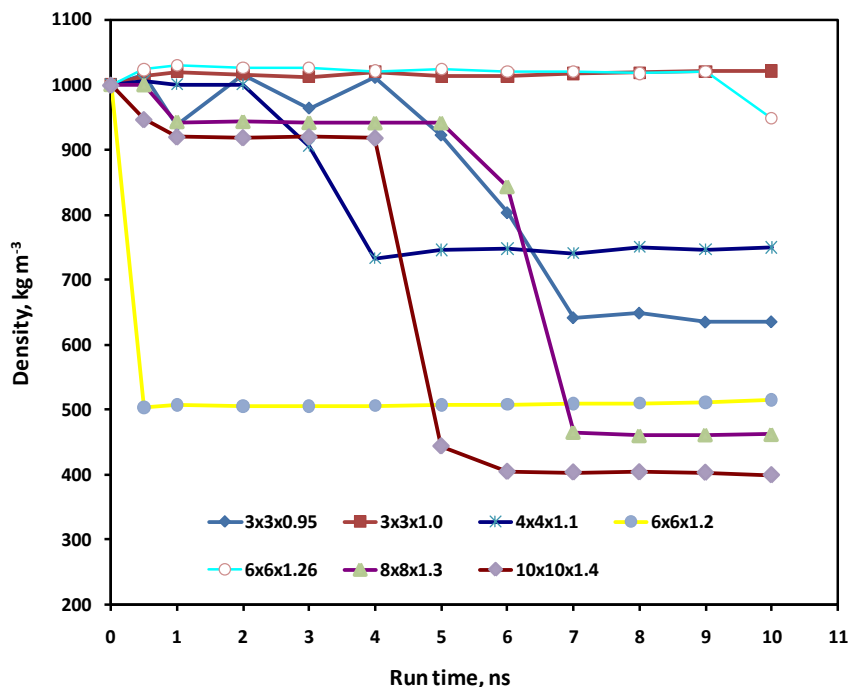


Figure 3 Computed density profiles of some films versus simulation run time.

To achieve a reasonable and consistent research approach, 1 ns was considered to be the CRT for a $4 \times 4 \times 1.10$ nm water film (see Figure 3-4). Following this principle, the CRT for a $4 \times 4 \times 1.05$ nm water film would be 2 ns. Figure 3-4 shows the profiles of density versus simulation run time. When the ratio $(L_x=L_y)/L_z$ was different, the final ruptured shapes of films (a series of films with the same $L_x=L_y$ [e.g., as shown in Figure 3-3]) could be different. For a given water film with a fixed size (e.g., see Figure 3-2), the ruptured shape could be estimated by changing the run time. For different water films, the ruptured shapes also differed. For example, it is not easy for a $4 \times 4 \times 1.10$ nm water film to turn into droplets even with a long run time. For some films (e.g., $4 \times 4 \times 1.30$ nm water film), a certain shape cannot be achieved because the film will not rupture within a limited run time. For a water film with an L_z close to or a slightly larger than its critical thickness (please see the Gibbs dividing range in Part 3.3), it is not easy for the liquid to break into droplets. If the value of the L_z is less than its critical thickness, the water film could break into droplets and then form an aggregate (could be also regarded as a droplet state).

From Figure 3-4, when L_z was close to the critical thickness (within the Gibbs dividing range; see Part 3.3) of the film, the density change was sensitive at the rupture point. For $3 \times 3 \times 0.95$ and $4 \times 4 \times 1.10$ nm water films, the final densities were between 600 and 800 kg m^{-3} within 10 ns; while, for $4 \times 4 \times 1.05$ (in Figure 3-3) and $10 \times 10 \times 1.40$ nm water films, the final densities were between 400 and 600 kg m^{-3} . The reason for this behaviour was explained before: when the $L_x=L_y/L_z$ value was different,

the ruptured shapes could be different, and so the density profile of the final stage was correspondingly different. From the data shown in the figures and the table cited thus far, we noted that, after the film ruptured and even at prolonged the run times, the density does not change much. It just fluctuates around an ultimately achieved value.

3.1.3 Classification of films based on their corresponding CRTs

From Table 3-1 and Figure 3-4, it can be seen that, for $4 \times 4 \times 1.10$ nm water film, the rupture time is approximately 4 ns. This kind of film could be stable for a short time. The $4 \times 4 \times 1.0$ and $6 \times 6 \times 1.2$ nm films actually could exist for a very short time, or they could rupture at the beginning. The $4 \times 4 \times 1.15$ and $3 \times 3 \times 1.0$ nm films as shown in Figure 3-3 and Figure 3-4, respectively, could have larger CRT values. When the CRT of a film were infinity (meaning that they will not rupture within a limited time), the film could be regarded as a “stable film”. When the film could have a very large CRT, the film was regarded to be a “critical film”, in which the Z-dimensional thickness would be between “thin film” and “stable film”. A “thin film” has a medium CRT lying between the CRTs of a “ruptured film” and a “critical film”. The thinnest film is the type that could rupture in a very short time, and it appears that this kind of film could rupture at the beginning of the film formation. We established the following classifications to distinguish the four types of films: ruptured film, thin film, critical film, and stable film.

Some films that are close to their critical thickness (at the Gibbs dividing range discussed in Part 3.3) had medium CRT values. If they had large CRT values, their density at the first 11 ns would be $\sim 1000 \text{ kg m}^{-3}$. From thermodynamics and the MD study, two stable states (see Part 3.3) are achieved for liquid films after long simulation run times. These stable states are observed in the results obtained from both experiments and MD simulations. One state is 100% (CRT = infinity), and the other is the ruptured film state. If a certain film has a CRT = A ($0 < A < \infty$), after running for a long time, the film could finally change into droplets.

3.2 The new criterion to define and determine the critical thickness

To determine the critical thickness, MD simulations for different thicknesses and film lateral dimensions at a given constant simulation run time were performed.

Table 错误!文档中没有指定样式的文字。 -2 Density of water films with $L_x=L_y=4$ nm, $L_z = 0.7$ to 1.3 nm and run time=2ns.

L_z , nm	0.7	0.8	0.9	1.0	1.1	1.2	1.3
Density, kg m^{-3}	464.68	493.10	533.64	613.30	1001.04	999.08	1000.49

Table 3-2 shows the results obtained with a selected run time of 2 ns. When calculating density, one could selectively collect certain periods from the whole run time. For the data presented in Table 3-2, durations ranging from 1000 to 2000ps were selected to collect data needed to calculate density. Therefore, for the results discussed below in Parts 3.3 and 3.4, data from the last 1 ns of the simulation were applied to calculate density.

Generally, if the density was lower than 900 kg m^{-3} , the film was not intact. From Table 2, when $L_z \leq 1.0$, the film was broken. Therefore, one should decide which value of thickness is the critical thickness. One method we used was to set a critical density standard to define critical thickness; for example, 800 kg m^{-3} could be selected as the critical rupture density standard. This means that, if the density was above 800

kg m^{-3} , the film could be considered to be unbroken. Therefore, for the film ($L_x = L_y = 4$) in Table 3-2, the critical thickness could be between 1.0 and 1.1 nm, so one could select 1.05 nm. This method based on the severity of the break associated with the density profile. This means that if one selects 600 kg m^{-3} as the critical rupture density, the critical thickness could be 0.95 nm.

Similarly, following the methodology described for CRT in Part 3.1, 90% was applied here as the user-selected density to identify the critical rupture point. Another method for defining the critical thickness would be to apply accurate dynamic phenomenon. From Table 3-2, the density did not change dramatically when $L_z \leq 1.0$; however, when $1.0 < L_z < 1.1$, the density changed dramatically (within the Gibbs dividing range discussed in Part 3.3). Therefore, if one arbitrarily chose 600 kg m^{-3} as the critical rupture density standard, the true dynamic phenomenon will not be reflected. Therefore, the value chosen for the critical density should always be within the Gibbs dividing range.

Using water film $L_x = L_y = 4$ as an example, the critical thickness can be between 1.1 and 1.0. When $L_x = L_y = 4$ and $L_z = 1.05 \text{ nm}$ and if the final density was above 900 kg m^{-3} , the critical thickness could be between 1.0 and 1.05 nm; if the final density was below 900 kg m^{-3} , the critical thickness could be between 1.05 and 1.10 nm. In fact, the critical thickness could be obtained more precisely by continuing to divide as shown above. The density changed considerably when the L_z was close to its critical thickness.

Comparing the definitions of CRT and critical thickness reveals that when the rupture occurs (in Part 3.3, CRT=A), then after that CRT time point or if the L_z changes a little bit, the film state changes dramatically, from unbroken to broken film states. For the definition of CRT (fixed film size) and with a prolonged time, the density exhibits a decreasing trend and fluctuates at a constant value at the final stages of the simulation. At critical film thickness (fixed time), the density decreases significantly at an L_z thickness (within the Gibbs dividing range) close to the critical thickness. The two parameters indicate that the system changes significantly at the critical points.

3.3 Correlation between the CRT and the critical thickness

To propose the Gibbs dividing area (i.e., the Gibbs dividing range) and the two stable film states, a typical plot of density versus thickness is shown in Figure 3-6.

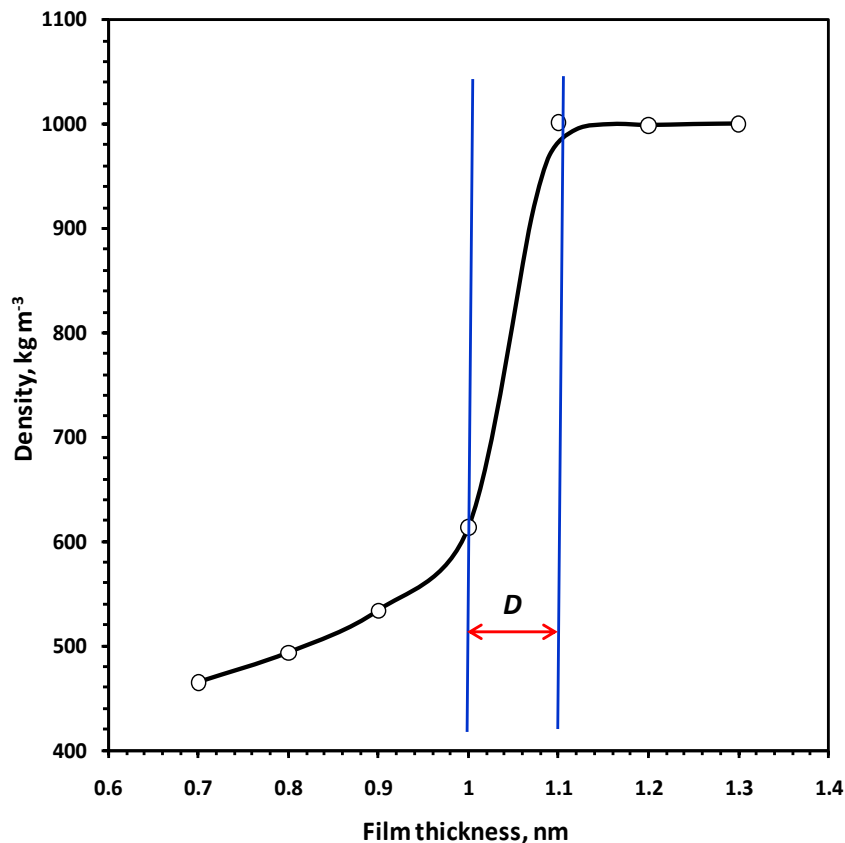


Figure 4 The illustrational plot of density versus film thickness to define Gibbs dividing surface range.

The term, D , is the Gibbs dividing range, $D = L_2 - L_1$, where L_2 and L_1 describe the film thicknesses of a density value of 100% and 60%, respectively. The Gibbs dividing range is the range $[L_1, L_2]$. When a film thickness L is within $[L_1, L_2]$, the film is not in its stable state. Only within the Gibbs dividing range, the CRT and critical thickness are sensitive to the change in the run time and film thickness. This Gibbs dividing range serves as a reference for interpreting results in Sections 3.1 and 3.2. If a film (the film size is fixed) has a plot similar to the plot in Figure 3-6, it has a $\text{CRT} = A$ ($0 < A < \infty$). If one film does not have a plot similar to Figure 3-6 (with a finite run time, between A and ∞), this type of film either has $\text{CRT} = \infty$ (at the right side of L_2) or a $\text{CRT} = 0$ (at the left side of L_1). When time is fixed, there are two stable film states. When the film thickness L is larger than " L_2 ," the density is 100%; when L is smaller than " L_1 ," the film forms droplets but is also in stable state.

From Figure 3-7, the plot will shift to the right side slightly when the run time increases. And for a given film, the Gibbs dividing range $[L_1, L_2]$ will change slightly, while its D value usually will not change significantly. Based on the knowledge that D changed very slightly, we plotted D versus the film lateral scale $L_x = L_y$ in Figure 3-8.

This showed that, when the $L_x = L_y$ became larger, its corresponding D value would gradually decrease. Generally, half of the Gibbs area is at 75 to 80% densities, which similarly conforms to the usual interface definition used in the literature.

3.4 Prediction of CRT and critical thickness

3.4.1 Prediction of CRT

CRTs and critical thicknesses of water films are provided in Tables 3-3 and 3-4, respectively.

Table 3 CRT of some water films.

Film dimensions ($L_x \times L_y \times L_z$), nm ³	CRT, ns
3×3×0.80	ruptured film
3×3×0.90	3
3×3×0.95	5
3×3×1.00	>10
4×4×1.00	ruptured film
4×4×1.05	2
4×4×1.10	4
4×4×1.15	>10
6×6×1.20	ruptured film
6×6×1.26	10
8×8×1.30	6
8×8×1.366	>10
10×10×1.40	5
10×10×1.50	>10

From Table 3-3, when the value of the lateral size ($L_x = L_y$) becomes larger, its associated CRT becomes more sensitive. When the lateral size is small (e.g., 3×3 nm), its thickness L has a larger range of D to have a medium CRT. However, when the $L_x = L_y$ is large, the same range of L could result in the CRT changing from zero (i.e., a ruptured film) to a very large CRT. This is similar to the trend of D versus the lateral dimension. From Table 3-3, it is not possible to predict CRT. Table 3-4 lists critical thicknesses of some water films versus time.

Table 4 Critical thickness (nm) of water films versus run time.

Time, ns	Lateral dimensions ($L_x \times L_y$), nm ²				
	3×3	4×4	6×6	8×8	10×10
1	0.85	1.04	1.20	1.27	1.32
2	0.87	1.05	1.20	1.27	1.33
3	0.90	1.07	1.22	1.28	1.35
4	0.92	1.09	1.23	1.29	1.37
5	0.94	1.10	1.24	1.30	1.40
6	0.95	1.11	1.26	1.31	1.41
7	0.96	1.11	1.26	1.33	1.42
8	0.96	1.12	1.26	1.36	1.44
9	0.97	1.13	1.27	1.37	1.45
10	0.99	1.14	1.27	1.37	1.45

Generally, when the lateral size is fixed, the critical thickness does not increase considerably with increasing run time. Figure 3-9 show a plot of critical thicknesses versus run time for 4×4 nm films, which serves as a typical example for predicting the CRT.

In Figure 3-9, the plot levels off over a prolonged run time. If the value of the L thickness is small (i.e., not in a stable state), its H-bonding network is not strong enough to keep the water molecules stable, so the film would tend to rupture over time. When the film is stable (CRT=0, droplet state; CRT= ∞ , always intact film), the cohesive force—H-bonding (H-bonding due to Coulombic-static force) can keep the water molecules in their equilibrium position, but the molecules can still vibrate and fluctuate slightly. It is obvious that, with increasing temperature, the molecules vibrate more rapidly, and the film becomes more likely to rupture and break into droplets. According to thermodynamic theory and MD simulation, the two final stable states result from the van der Waals force and the Coulombic-static force. By fitting this plot, an equation is obtained as follows: $L = -0.21874^{-0.0662CRT} + 1.25$, where the film thickness is nm and the CRT is in ns.

3.4.2 Prediction of critical thickness

Critical thicknesses of the water films are provided in Table 3-4. The plot of critical thickness versus the reciprocal of corresponding run time, $1/t$, is shown in Figure 3-10 using data from Table 3-4.

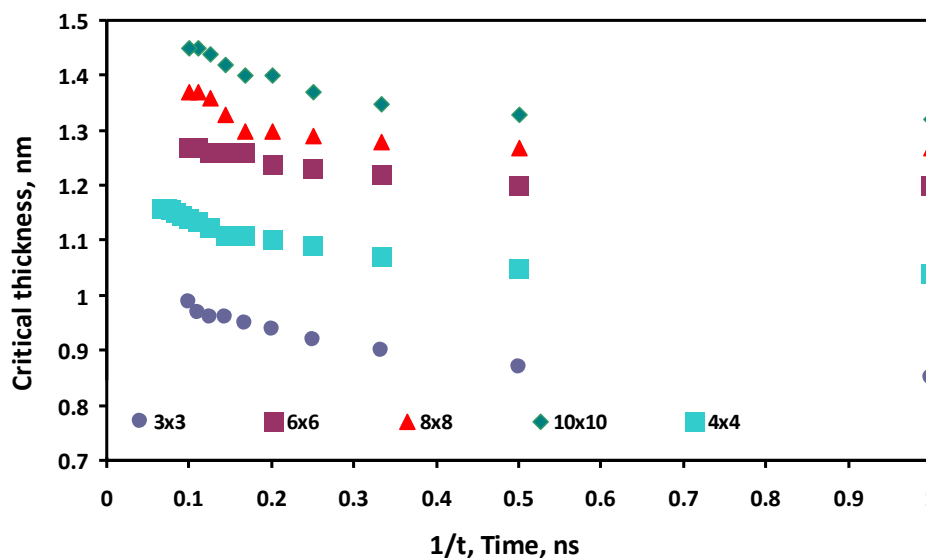


Figure 5 Computed critical film thickness versus reciprocal of its run time (ns), $1/t$.

From Figure 3-10, prolonging the run time allows the critical thickness to converge. A final critical thickness can be determined through data fitting when the run time approaches infinity. With a prolonged run time, the trend would level off (see the 4×4 and 8×8 nm films in Figure 3-10). Here, the $1/t$ value is too narrow to see the trend.

3.5 Effect of ions on film rupture

The simulation run time was 3 ns for the films with ions. The thinner (e.g., $3 \times 3 \times 0.8$ nm) film was ruptured, and the thicker (e.g., $3 \times 3 \times 1.0$, $4 \times 4 \times 1.15$, $6 \times 6 \times 1.3$ nm) water film was unbroken. These films were used as references to study the effect of ions on the film rupture. Here, eight ions (eight Na^+ and eight Cl^- ions) were added to 3×3 , 15 ions to 4×4 nm films, and 30 ions to 6×6 nm films. Table 3-5 shows the states of film after running for 3 ns.

From the results for $3 \times 3 \times 1.0$, $4 \times 4 \times 1.15$ and $6 \times 6 \times 1.3$ nm films, it can be concluded that Na^+ and Cl^- ions do not break the films. It means that the presence of NaCl does not have an adverse effect on the nanofilm instability. Based on experimental results, the NaCl ion effect on the film stability is weak because sodium and chloride ions are small and, therefore, are strongly hydrated, forming strong ion pairing within the film. However, comparing with big ions and molecules such as surfactants, e.g., sodium dodecyl sulfate, the NaCl salt ions are not strong in stabilizing water films. The salt can only slightly influence the transient stability of the films, which can be important in the flotation separation of hydrophobic particles.

To investigate the effect of ions on a film thickness L close to the critical thickness (within the Gibbs dividing range), a $5 \times 5 \times 1.14$ nm water film running for 11 ns was applied as reference. This water film ruptured at 4300 ps. By adding 22 NaCl ions, the $5 \times 5 \times 1.14$ nm film ruptured at 4350 ps. This comparison shows that NaCl does not have a remarkable effect on film rupture. The TIP4P water model also was applied to study the effect of ions. The simulation run time for the $3 \times 3 \times 1.0$ nm TIP4P water film was 4 ns, and the water film was intact throughout the simulation. Eight Na^+ and Cl^- ions then were added to the water film, and again, the water film was intact after the 4-ns run time..

4 Conclusions

MD simulations of film rupture processes were performed to determine if general predictions of the CRT and critical thickness of water films could be achieved. The CRT is an important parameter when applied to large-scale simulations, and its determination by simulation could be used to assist experimental efforts. The proposal of this new criterion can shed light on the correlation between the rupture process and thermodynamic properties. The combination of MD simulation of films and Gibbs dividing ranges is a new interpretation for film and interface related research. Overall, NaCl ions have an effect on the stability of films but the effect is significantly weaker when compared with surfactants. In the future, we could use large-scale MD simulations to investigate the process, which will take into account all the environmental factors and should be able to reproduce this phenomenon better.

Acknowledgements

References

1. Henry Christine, L., et al., *Ion specific electrolyte effects on thin film drainage in nonaqueous solvents propylene carbonate and formamide*. Langmuir, 2009. **25**(17): p. 9931-7.
2. Karakashev, S.I., E.D. Manev, and A.V. Nguyen, *Effect of double-layer repulsion on foam film drainage*. Colloids Surf., A, 2008. **319**(1-3): p. 34-42.
3. Karakashev, S.I., et al., *Effect of ionic surfactants on drainage and equilibrium thickness of emulsion films*. J. Colloid Interface Sci., 2008. **318**(2): p. 358-364.

4. Karakashev, S.I. and A.V. Nguyen, *Effect of sodium dodecyl sulphate and dodecanol mixtures on foam film drainage: Examining influence of surface rheology and intermolecular forces*. Colloids Surf., A, 2007. **293**(1-3): p. 229-240.
5. Karakashev, S.I. and A.V. Nguyen, *Do Liquid Films Rupture due to the So-Called Hydrophobic Force or Migration of Dissolved Gases?* Langmuir, 2009. **25**(6): p. 3363-3368.
6. Karakashev, S.I., A.V. Nguyen, and E.D. Manev, *A novel technique for improving interferometric determination of emulsion film thickness by digital filtration*. J. Colloid Interface Sci., 2007. **306**(2): p. 449-453.
7. Karakashev, S.I., et al., *Anomalous Ion Effects on Rupture and Lifetime of Aqueous Foam Films Formed from Monovalent Salt Solutions up to Saturation Concentration*. Langmuir, 2008. **24**(20): p. 11587-11591.
8. Manev, E.D. and A.V. Nguyen, *Effects of surfactant adsorption and surface forces on thinning and rupture of foam liquid films*. Int. J. Miner. Process., 2005. **77**(1): p. 1-45.
9. Manev, E.D. and A.V. Nguyen, *Critical thickness of microscopic thin liquid films*. Adv. Colloid Interface Sci., 2005. **114-115**: p. 133-146.
10. Nguyen, A.V., et al., *Dewetting kinetics on silica substrates: Three phase contact expansion measurements for aqueous dodecylammonium chloride films*. Miner. Eng., 2006. **19**(6-8): p. 651-658.
11. Nguyen Phong, T. and V. Nguyen Anh, *Drainage, rupture, and lifetime of deionized water films: effect of dissolved gases?* Langmuir, 2010. **26**(5): p. 3356-63.
12. Qu, X., et al., *Anomalous thickness variation of the foam films stabilized by weak non-ionic surfactants*. J. Colloid Interface Sci., 2009. **337**(2): p. 538-547.
13. Taran, E., et al., *Anomalous Time Effect on Particle-Bubble Interactions Studied by Atomic Force Microscopy*. Langmuir, 2009. **25**(5): p. 2797-2803.
14. Tsekov, R., et al., *Streaming Potential Effect on the Drainage of Thin Liquid Films Stabilized by Ionic Surfactants*. Langmuir, 2010. **26**(7): p. 4703-4708.
15. Hampton, M.A. and A.V. Nguyen, *Nanobubbles and the nanobubble bridging capillary force*. Adv. Colloid Interface Sci., 2010. **154**(1-2): p. 30-55.
16. Zimmerman, W.B., V. Tesař, and H.C.H. Bandulasena, *Towards energy efficient nanobubble generation with fluidic oscillation*. Curr. Opin. Colloid Interface Sci., 2011. **16**: p. 350-356.
17. Radoev, B., et al., *Wetting film dynamics and stability*. Colloids Interface Sci. Ser. , 2007. **3**(Colloid Stability and Application in Pharmacy): p. 151-172.
18. Ajaev, V.S., *Effect of nanoscale bubbles on viscous flow and rupture in thin liquid films*. Physics of Fluids, 2006. **18**(6): p. 068101/1-068101/4.
19. Nguyen, A.V. and H.J. Schulze, *Colloidal science of flotation*. 2004, New York: Marcel Dekker. 840.
20. Baer, M., et al., *Interpreting vibrational sum-frequency spectra of sulfur dioxide at the air/water interface: a comprehensive molecular dynamics study*. J Phys Chem B, 2010. **114**(21): p. 7245-9.
21. Dang, L.X., *Computational Study of Ion Binding to the Liquid Interface of Water*. J. Phys. Chem. B, 2002. **106**(40): p. 10388-10394.
22. Dang, L.X., *Computational studies of ions at interfaces of hydrogen bonded liquids*. Abstracts of Papers, 229th ACS National Meeting, San Diego, CA, United States, March 13-17, 2005, 2005: p. PHYS-108.

23. Dang, L.X. and B.C. Garrett, *Molecular mechanism of water and ammonia uptake by the liquid/vapor interface of water*. Chem. Phys. Lett., 2004. **385**(3,4): p. 309-313.
24. Dang, L.X. and B.M. Pettitt, *Chloride ion pairs in water*. J. Am. Chem. Soc., 1987. **109**(18): p. 5531-2.
25. Dang, L.X. and B.M. Pettitt, *A theoretical study of like ion pairs in solution*. J. Phys. Chem., 1990. **94**(10): p. 4303-8.
26. Dang, L.X., B.M. Pettitt, and P.J. Rossky, *On the correlation between like ion pairs in water*. J. Chem. Phys., 1992. **96**(5): p. 4046-7.
27. Dang, L.X., et al., *Molecular Simulation Analysis and X-ray Absorption Measurement of Ca²⁺, K⁺ and Cl⁻ Ions in Solution*. J. Phys. Chem. B, 2006. **110**(47): p. 23644-23654.
28. Mucha, M., et al., *Unified Molecular Picture of the Surfaces of Aqueous Acid, Base, and Salt Solutions*. J. Phys. Chem. B, 2005. **109**(16): p. 7617-7623.
29. Sun, X., C.D. Wick, and L.X. Dang, *Computational Studies of Aqueous Interfaces of SrCl₂ Salt Solutions*. J. Phys. Chem. B, 2009. **113**(42): p. 13993-13997.
30. Berendsen, H.J.C., D.v.d. Spoel, and R.v. Drunen, *GROMACS: A message-passing parallelmolecular dynamics implementation*. Comp. Phys. Comm., 1995(91).
31. Hess, B., et al., *GROMACS 4: Algorithms for highly efficient, load-balanced, and scalable molecular simulation*. J. Chem. Theory Comput., 2008(4): p. 435-447.
32. Lindahl, E., B. Hess, and D.v.d. Spoel, *GROMACS 3.0: A package for molecular simulation and trajectory analysis*. J. Mol. Mod., 2001(7): p. 306-317.
33. Spoel, D.v.d., et al., *GROMACS: Fast, Flexible and Free*. J. Comp. Chem., 2005(25): p. 1701-1719.